Journal of Theoretical and Applied Information Technology
31st March 2025. Vol.103. No.6

ISSN: 1992-8645 www.jatit.org E-ISSN: 1817-3195

# DEEP LEARNING-BASED CLASSIFICATION AND SEGMENTATION OF CHEST PATHOLOGIES

**JAKKULA SRAVANTHI[1], BANDA VENKATA RAMANA[2], JUTHUKA ARUNA DEVI[3], SURAGALI CHANTI[4,*], SRADHANJALI PATTANAIK[5], PALTHIYA ANANTHA RAO[6], MARADA SRINIVASA RAO[7]**

[1]Department of Information Technology, VNR Vignana Jyothi Institute of Engineering and Technology, Hyderabad, Telangana, India

[2]Department of Computer Science and Engineering, Vignan's Institute of Information Technology(A), Visakhapatnam, Andhra Pradesh, India

[3]Department of Computer Science and Engineering (AI&ML, DS), Anil Neerukonda Institute of Technology and Sciences (A), Visakhapatnam, Andhra Pradesh, India

[4]Department of Computer Science and Engineering, GMR Institute of Information Technology(A), Rajam, Andhra Pradesh, India

[5]Department of Computer Science and Engineering, Vignan's Institute of Engineering for Women (A), Visakhapatnam, Andhra Pradesh, India

[6]Department of Computer Science and Engineering, Koneru Lakshmaiah Education Foundation, Green Fields, Vaddeswaram, Andhra Pradesh, India

[7]Department of Information Technology, MVGR College of Engineering (A), Vizianagaram, Andhra Pradesh, India

E-mail: sravs521@gmail.com[1], bvramana2005@gmail.com[2], jarunadevi2003@gmail.com[3], sunchanti@gmail.com[4,*], sradhanjali.pattanaik@gmail.com[5], pananth534@kluniversity.in[6], srinivas.marada22@gmail.com[7]

**ABSTRACT**

Chest diseases, such as COVID-19, viral pneumonia, and lung opacity, in most severe cases, call for quick diagnosis and accurate treatment. Applying deep learning methods, mainly convolutional neural networks (CNNs), has become attractive among machine learning techniques for automated image diagnostics. This paper reports a new ensemble approach that utilizes CNN-1, CNN-3 and VGG-16 structures to classify the disease and U-Net for segmenting the chest diseases in X-ray pictures considered from the Kaggle repository. Data augmentation is applied to original samples to increase the size and performance of a model. The segmentation procedure shows a high capability to define interested regions in the lung, which contributes to higher accuracy, performed comparison between the proposed segmentation method and existing methods. The following results obtained by the model are 96% in segmentation and 87.7% in classification- reflecting the preferred method's high accuracy. The proposed model was evaluated on performance metrics like F1-score, Precision, and Recall. Therefore, this result may lead the way for enhanced diagnostic accuracy and treatment decisions in clinical settings.

**Keywords:** *Viral Pneumonia, COVID-19, Lung Opacity, Deep Learning, Ensemble, CNN-1, CNN-3, VGG 16, Segmentation, U-Net.*

## 1. INTRODUCTION

Lung illness includes considerable stress connected with global health systems and society [1-4]. Due to its nature of spread, it affects people no matter who or where they come from. This research paper will primarily describe communication about the reasons for these disorders, such as COVID-19, viral pneumonia, and lung opacity. Lately, these diseases have become household terms after they gained considerable attention worldwide because of their impact on health status. COVID-19, since it is this novel coronavirus SARS-CoV-2, probably the origin of 2019, has come to stay as a global pandemic has spread incredibly fast, leaving the world to deal with millions of suspects and many deaths [5-7]. The illness majorly impacts the airways, resulting in high-grade fever, respiratory symptoms, and shortness of breath. So, the worst cases of a respiratory disease known as COVID-19 may require ventilator support in intensive care. Viral pneumonia is also an essential aspect of the respiratory system. It differs based on infection caused by viral agents, such as influenza, adenovirus, or respiratory syncytial virus (RSV). It manifests by cough, fever, and shortness of breath symptoms, mimicking bacterial pneumonia.

A worsening degree of lung opacity manifested as an increase in the density of a certain area on chest radiographs, such as chest X-rays or CT scans, is the result of the slow accumulation of fluid or scar tissue within air spaces [8]. The chest X-ray radiographs show viral pneumonia with symmetric peripheral patchy opacities and an absent or reverse hilum with a predilection for the lower lobes.

*Figure 1: Normal Lungs*

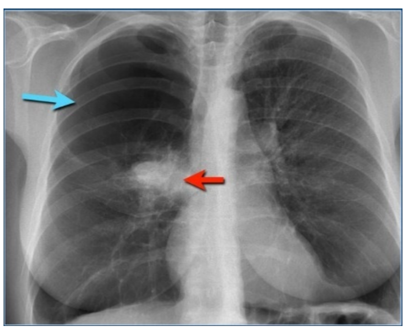

*Figure 2: Affected Lungs*

The above Figures 1 and 2 represent a patient x-ray standard lung image and an affected disease lung image. By deploying deep learning algorithms like segmentation and classification, scientists can hone predictive models that can differentiate various chest sickness patterns by their associated radiograms. This work likely will help improve robust, widespread deep-learning systems for detecting and preventing lung-related diseases, such as lung opacity, COVID-19, and viral pneumonia. It could also be very helpful in managing the fallout of those diseases on general public health.

## 2. LITERATURE SURVEY

V.K Singh et al. [9] provide a deep model that integrates manual features with DCNN's technology to diagnose ten diseases, including COVID-19, accurately. Segmenting the lung images employing Info-MGAN implementation and, with the help of ORB and SURF important points extractors, enabled the considered strategy to attain a very high accuracy (98.20% via VGG-19 and ORB).

J. Liu et al. [10] proposed a new method, a two-phase cross-domain with a transfer learning framework for detecting COVID-19 and segmentation viruses with the help of CT pictures. This study included the nCoVSegNet model for segmentation, which considers a feature fusion technique called attention-aware feature fusion.

Chauhan et al. [11] apply a depthwise convolution with optimizations and a wavelet-based multiresolution analysis to recognize COVID-19 automatically from x-ray images related to the chest. The four models taken into account from DL are Deep GRU-CNN, Coro Net, LMNet, and CVDNet, which were introduced in this study. This new proposed model obtained 99.47% on training & 98.91% on testing accuracies, respectively. In addition to accuracy, some metrics, such as outcomes, are precision-98%, recall-98%, specificity-99%, and f1-score-98%, respectively.

Asghar et al. [12] suggested a Depth wise Separable Convolution Neural Network using Conv2D layers with a base of MobileNet named (DWS-based MobileNet) to identify masks in facial images. Performed comparison analysis between this novel and existing method, the DWS-based MobileNet given better performance considered, and their outcomes are (Acc. = 93.14, Pre. = 92, recall = 92, F-score = 92).

Maheswari et al. [13] demonstrated a robust TB identification method utilizing deep learning algorithms implemented onto cX-ray images. This paper presented an idea with normalized images, data augmentation, and transfer learning with segmentation techniques based on nine different CNN models, including DenseNet201 and ChexNet, which increase accuracy in automatically categorizing TB and normal chest radiographs. The accuracy of DenseNet201 hit the impressive mark of 98.6%.

Saood and Hatem [14] presented two deep learning segmentation models called SegNet to form a network, and U-NET is a tool for segmentation. Both differ in structural behaviour and masked infected areas of CT lung scans. These were effectively used on binary and multi-segment classification. To educate the model, 72 data images were used, 18 were tested, and validation was done on 10 images. The utilized network successfully classified infected and non-infected areas compared to existing methods. Nearly 95% accuracy was achieved, and the U-Net tool obtained good outcomes on multi-class segments with 91% accuracy.

Sun et al. [15] first instigated computer tomography pictures related to COVID-19 wounds with segmentation using swin-UNet. Such a network allows a solution to problems including, for example, multi-scale segmentation and uneven grey distribution. This paper offers three innovations: the novel DF loss function (DF) for fine target segmentation, the URIM module (uncertain region inpainting) for segmentation refinement, and the ResMLP module (a residual transformer) for feature conservation. It delivers better outcomes (Dice: model achieved an accuracy of (0.812, 0.780, 0.848, 0.683 (Precision, Recall, IOU)). Al-Masni and Kim [16] used chest X-ray (CXR) pics for CVOV (COVID-19 virus) diagnosis, paying great attention to the model technique and dataset. The article presents CMM-Net (Contextual Multi-Scale Multi-Level Network), which includes segmentation and convolutional neural networks with the ISIC 2017 dataset, which have skin-related dermoscopy segmented images, DRIVE segmentation on blood vessels related to fundus images and BraTS 2018 are MR scans for Brain segmentation dataset. Apart from this, augmentation used in testing is referred to as Inversion Recovery (IR), which takes into account the operators of logical “OR” and “AND”. The proposed models present 85.78% skin, 80.27% blood vessel, and 88.96% brain segmentation.

Vasilev et al. [17] promote that approach, which enhances the credibility of AI diagnosis by creating annotated lesion CXRs from the annotated lesion and normal CXRs. Evaluating ChestX-Det10 and RSNA datasets leads to a mere 4% improvement. Their approach improves overall detection model effectivity, especially that of faster RCNN, through correcting class imbalance and augmenting training data.

Sahin et al. [18] announced the Mask R-CNN-based COVID-net project to highlight GGOs in chest CT scans of COVID-19 patients. Its positive % recognition rate of 98.25% in instance segmentation makes it a powerful ally for RT-PCR testing, helping the sorting and verification process. This approach is outstanding because early detection is crucial since the strain the pandemic is putting on public health is overwhelming.

Ippolito et al. [19] utilized a dataset integrated with three sub-datasets: 1. COVID-19+ with 1140 samples, 2. bacterial pneumonia with n = 500 and 3. healthy patient data with 1000 samples. The obtained confusion matrix evaluated TP, TN, FP, and FN data with 95% TP obtained. The outcome of the three sub-datasets are COVID-19+ coefficient of κ is 0.822 and pneumonia+ κ is 0.913). 96% sensitivity and 79.8% specificity for COVID-19+ and 94.7% sensitivity and 80.2% specificity for bacterial pneumonia. The system achieved 93.8% precision, with a misclassification rate of 6.2% in detecting COVID+, pneumonia+, and healthy subjects.

Fung, Liu et al. [20] argued that they designed an Inf-Net neural network to recurrently segment COVID-19 lung infections automatically from the battlefield of chest CT scans. It expects the infected areas and uses reverse attention modules and a parallel partial decoder to find them. Using the self-supervised method, their two-stage segmentation accuracy is increased by gaining from unlabeled input. The result obtained by the F1-score is the best score for self-supervised, 0.63, compared to baseline models, 0.55 and 0.49.

Badrinarayanan et al. [21] applied semantic segmentation and a CNN named Seg-Net, developed by researchers as their deep learning model to detect CD before it develops into a severe problem. According to them, this proposed technique can classify lung ailments individually through pixel-wise analysis and an encoder-decoder network. The method gets the desired results with aids like contouring and grayscale conversion with the help of the pres processing techniques. The trick resolves the contamination issues in CT scans by using aids like contouring and grayscale conversion with the help of pre-processing techniques.

Alam et al. [22] include many complete discriminators and a generator that looks like a U-net and is conditioned on a radiograph target image. The generator reaches a 97.4% mean dice score in its attempt to segment lung masks under input CXR images. A discriminator block is an essential element of the model that has been developed and generates binary classification. Similar to a U-net, the model is a generator conditioned using X-ray imaging as input but also involves multi-level discriminators. The generator has learnt to create a lung segmented mask by using as input CXR pictures, attaining a mean dice score of 97.4%.

clients encrypt the data until it is stored in the cloud. Cryptonite is a secure repository of storage available on Cloud that addresses these problems by a strongbox mannequin for shared key administration. The author describes Cryptonite as a service for computing device customer that discuss efficiency and optimum utilization of

Journal of Theoretical and Applied Information Technology
31st March 2025. Vol.103. No.6

ISSN: 1992-8645 www.jatit.org E-ISSN: 1817-3195

resources, and furnish an empirical evaluation of upgrades [30].

Wu et al. [23] proposed a BIased Multi-Head Attention Vessel Net (IBIMHAV-Net), which enlarges a 3D-swin-transformer worked on merging uo of convolutional layer and selt attention layers. The whole implementation can be done using the 3DIRCADb dataset. The novel model achieved 74% dice and 77% sensitivity on the test part.

Saha et al. [24] considered grey materialized density, which means Ground-glass opacity (GGO) of CT lung images is an authentic feature for predicting COVID-19. This study aimed at the morphology of images, segmentation, and designs involved in GGO. MosMedData: 1110 lung scans with and without infected images of CoV. PointNet++ found GGOs in images with a high accuracy metric of 98%. IoU 92%.

Saha et al. [24] considered grey materialized density, which means Ground-glass opacity (GGO) of CT lung images is an authentic feature for predicting COVID-19. This study aimed at the morphology of images, segmentation, and designs involved in GGO. MosMedData: 1110 lung scans with and without infected images of CoV. PointNet++ found GGOs in images with a high accuracy metric of 98%. IoU 92%.

Gunraj et al. [25] introduced a new system named COVIDNet-CT, which is DeepN Net Approach. To prevent the problems raised in earlier studies, which are difficult to identify COVID-19-infected patients using CT scans due to other lung-related conditions. Furthermore, this research comprised COVID-19-CT, a dataset collected from China National Center for Bioinformation with 104,009 images over 1,489 subjects, which is an open-access dataset—performed a comparison analysis among ResNet-50, NASNet-A-Mobile, EffiecientNet-B0 and COVIDNet-CT, the proposed model achieved 99% accuracy with 1.40 million parameters.

Kim et al. [26] introduced a Deep learning system with four-region segmentation applied first to the disparate right and left parts of the lungs, and for disease, detection, served an ensemble approach with five Deep models. The proposed method contrasts with the radiographic assessment of the quality of lung oedema (RALE) interpreted by doctors. The four-region segmentation of each scan is obtained by mean-average intensities, which specify correlation as +ve based on the RALE.

Afshar P et al. [27] generated a COVID forecasting model based on the CXR image. A new system called COVID-CAPS outperforms previously deployed Deep Learning models in terms of performance. A few metrics are taken into consideration in order to measure the performance of COVID-19: accuracy of 96%, specificity of 96%, and sensitivity of 90%. Less trainable factors are also taken into consideration.

A. I. Khan et al. [28] examined a method combining transfer learning and Xception that takes into account two multi-class classification efforts. 1. Three classes with labels that separate COVID-19 from viral and bacterial pneumonia from controls 2. Pneumonia versus COVID-19 versus controls. Sampling approaches under sampling were used on distributed images across four labelled groups in order to address the issue of imbalanced data: 327 viral pneumonia, 330 bacterial pneumonia, 290 COVID-19, and 310 control CT scans of the chest. Two multi-class datasets were used to test the model; with three classes, an accuracy of 94 was reached, and with four classes, an accuracy of 89. In addition to this, a three-class cross-database yielded an extra 90 accuracy.

Afshar et al. [29] presented a novel ML architecture named Capsule Network, which avoids the limitations of CNN. This research focused on four goals: 1. It must prevent the overfitting issue. 2. Capsule Net must detect brain tumour classification. 3. A segment of the tumour must be explored using MRI scans. 4. Visualization graphs must be implemented to understand the outcome of Capsule Net quickly.

Bhalla et al. [30] utilizes radiographs to predict various diseases. These are mainly used to find several patterns in radiographs 1. Peripheral Airspace Opacities, which present lower lobe. 2. GGO: Ground Glass Opacity provides an easier way of detecting infected lung areas. 3. Peribronchial Consolidation focused on the middle part and lower lobe to find infections. 4. Multifocal Airspace Opacities/GGO, same as 2nd pattern, doesn't present bacterial and lower lobe infections. 5. Large Nodule or "Mass-Like" Opacities, which coexistence with other patterns.

Ye et al. [31] instigated a new system that comprises ML+DL techniques using demographic data, blood bio-data, and clinical scans to foresee COVID-19. The ensemble with the multi-level stacked framework proposed and, in addition, included CAM, LIME, and SHAP as XAI to predict COVID-19 collected the dataset from Manipal and custom-made from India. 1D-CNN was considered. The multi-level stacked algorithm attained 96% accuracy as the primary metric. It

Journal of Theoretical and Applied Information Technology
31st March 2025. Vol.103. No.6

ISSN: 1992-8645 www.jatit.org E-ISSN: 1817-3195

gained 94%, 95%, and 94% precision, recall and f1-score, respectively.

Teixeira et al. [32] performed a morphological segment-UNet CNN framework for image segmentation, and base CNN with Inception, ResNet-50, and VGG was utilized for

| Set | COVID-19 | Normal | Lung Opacity | Viral Pneumonia |
|---|---|---|---|---|
| Train | 2366 | 8039 | 3801 | 912 |
| Validation | 772 | 1499 | 1501 | 256 |
| Test | 478 | 654 | 710 | 177 |
| Total | 3616 | 10,192 | 6012 | 1345 |

classification. This study integrated with a three-class database: normal, lung opacity (pneumonia), and COVID-19. The segmentation attained two scores that were very helpful in segmenting the images: Dice coefficient: 0.98 and Jaccard distance: 0.034. The classification obtained 83%, spotting the disease with a multi-class f1-score of 88%.

Thimoteo et al. [33] considered two main attributes, pathogen and blood test (white blood cells are essential), to forecast the COVID-19 disease with AI approaches. Two combined models were utilized: logistic regression + boosting machine, called glass-box models, and random forest + support vector machine, called black-box models. The combined glass and black-box model achieved performance in terms of AUC 87%.

## 3. PROPOSED WORK

Dataset Description:

The COVID-19 Chest Radiography Database included in the study is the overall database for the classification of chest diseases. It concentrated on cases related to lung opacity, COVID-19, and viral pneumonia, regular instances. The dedicated dataset consists of 21,165 chest X-ray Images with four classes.

- COVID-19: The image set consists of the chest X-rays of 3616 confirmed patients with a COVID-19 diagnosis. The images were obtained from multiple data sources, such as public archives, the Internet, and scientific reports.

- Normal: There are 10,192 chest X-ray images in the Normal class, representing normal cases. The chest X-rays were obtained from three different repositories, thus covering normal chest X-ray datasets from diverse and complete settings.

- Lung Opacity: The Lung Opacity package has 6012 chest X-ray images that can be used to identify lung opacity conditions that are not COVID-related non-pulmonary lung infections. These images were obtained from a particular dataset, the Radiological Society of North America (RSNA CXR).

- Viral Pneumonia: The chest X-ray set for viral pneumonia contains 1345 images marking cases of the condition. These radiographs were picked from a committed database, the Chest X-ray website.

*Table 1. Dataset distribution broken as training, verification, and test.*

The above table gives the distribution of images among four labelled classes. The second class is named the regular class, which has the highest instances, and then the Lung Capacity class, which is almost double the disease indication class. The remaining two are the third and fourth largest sizes of the COVID-19 and Viral Pneumonia classes, respectively.

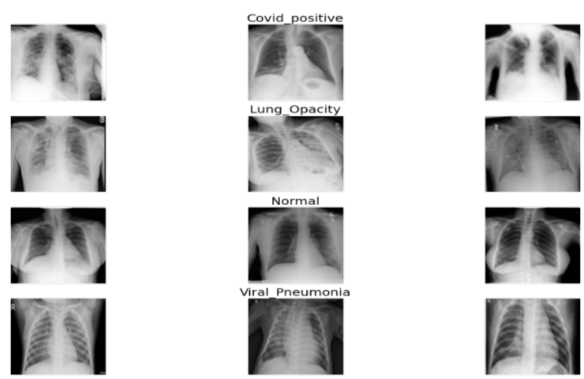


*Figure 3: Examples of Chest X-Ray images allied to four classes*

**Journal of Theoretical and Applied Information Technology**
31st March 2025. Vol.103. No.6

ISSN: 1992-8645 www.jatit.org E-ISSN: 1817-3195

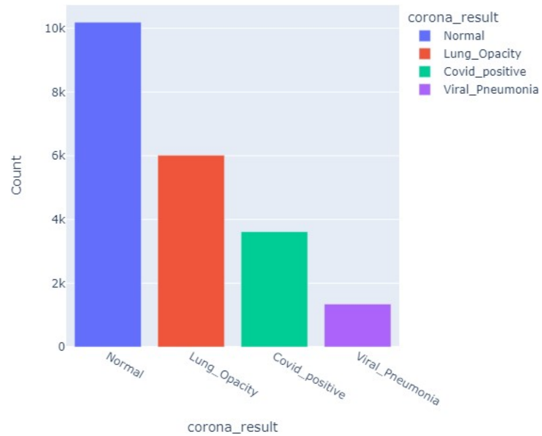


*Figure 4: The count plot shows value counts for a categorical target variable*

The standard deviation (std) and mean (average) of image samples can be very useful for determining the dataset details, pattern identification, and correlation between two values.

- If the scatter charts appear as a high amount of deviation among the samples, it may indicate that the dataset is highly heterogeneous and may require additional pre-processing or normalization.
- If the scatter plot shows little variance in the mean values of the samples, this indicates that the considered sample set is more homogeneous and easier to work with.
- If the scatter plot shows little variance in the mean values of the samples, this indicates that the considered sample set is more homogeneous and easier to work with.

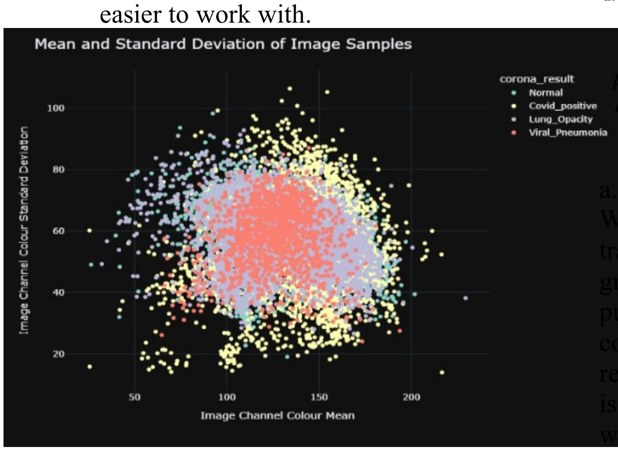


*Figure 5: Shows the importance of the standard deviation and mean of samples*

The above Figure 5 represents the scatter plot for the medial and standard deviation of four classes of target attributes, giving a detailed data distribution.

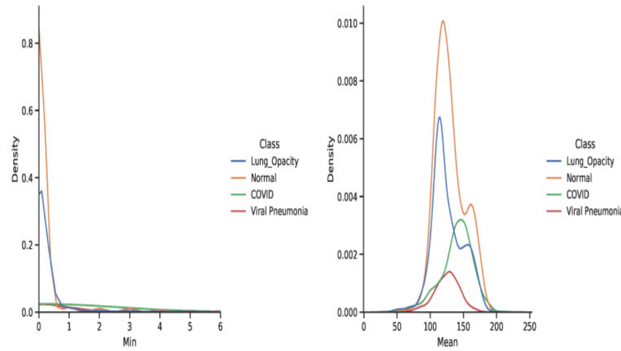


*Figure 6: Represents the MIN and medial distribution of RGB colour intensity for the four classes.*

**Pre-processing**

Data Augmentation:

We can alter already-existing photos in different ways to provide new training data. Expanding the amount of training data available may aid in enhancing machine learning models' performance, which is especially helpful when working with tiny or imbalanced datasets.

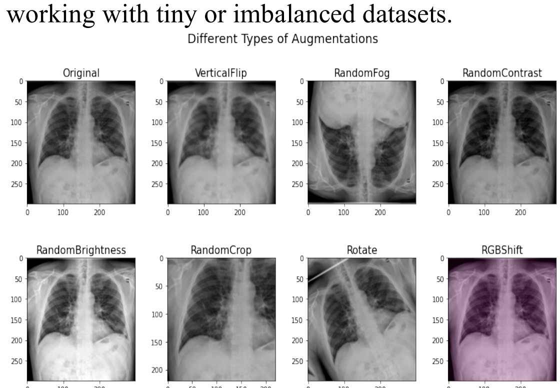


*Figure 7: Represents examples of CXR images after performing data augmentation techniques like Vertical Flip, Contrast, Crop, Brightness, degree Rotation, and Image colorization with RGB.*

a. Image Colorization

We have proposed that to utilize RGB image pre-trained models like the VGG16 network, our grayscale chest X-ray images were pre-processed in pursuit of the colorization goal. This stage aimed to convert the input monochrome images of high resolution to a three-channel RGB format since this is what the designed model for backpropagation would need. As we proceeded in our implementation, the imaging convert (RGB) function was used as part of this transformation on all our grayscale images. As a result, the grayscale image sequence is converted into a full "RGB" structure through experimental estimation of values for the channels separately, thus providing pseudo-color representation.

b. Image Resizing

Resizing images is a ubiquitous pre-processing step and is especially useful for image segmentation, object recognition, and classification problems for which machine learning is necessary. Resizing helps with two things: one, it meets the dimensional requirements of the model's architecture, and two, it reduces the amount of data and the complexity of processing, among many other advantages. Creating an image that is, say, 128 by 128 pixels in size will not only reduce the model's complexity but also cut down on computation power. Thus, the model will be more effective, taking into account the simple ideology that in lesser complexity, training times and memory needs will decrease.

c. Normalization

Default image normalization, commonly performed concurrently with scaling, is one more integral preparation step in handling image data. The normalization process implies bringing an image's pixel values into agreement with the shared scale or range, contributing to models' metrical training improvement or models' working of arrays. For the usual transform photos, all pixel values are within a specified range, which guarantees normalizing. Due to the contraction process, normalization reduces the estimates of the input values and can also accelerate the process of its convergence. By preventing the instability in the training process caused by large input values, getting it right is achieved.

Min-Max Normalization $x_{norm} = \frac{x - x_{min}}{x_{max} - x_{min}}$ … (1)

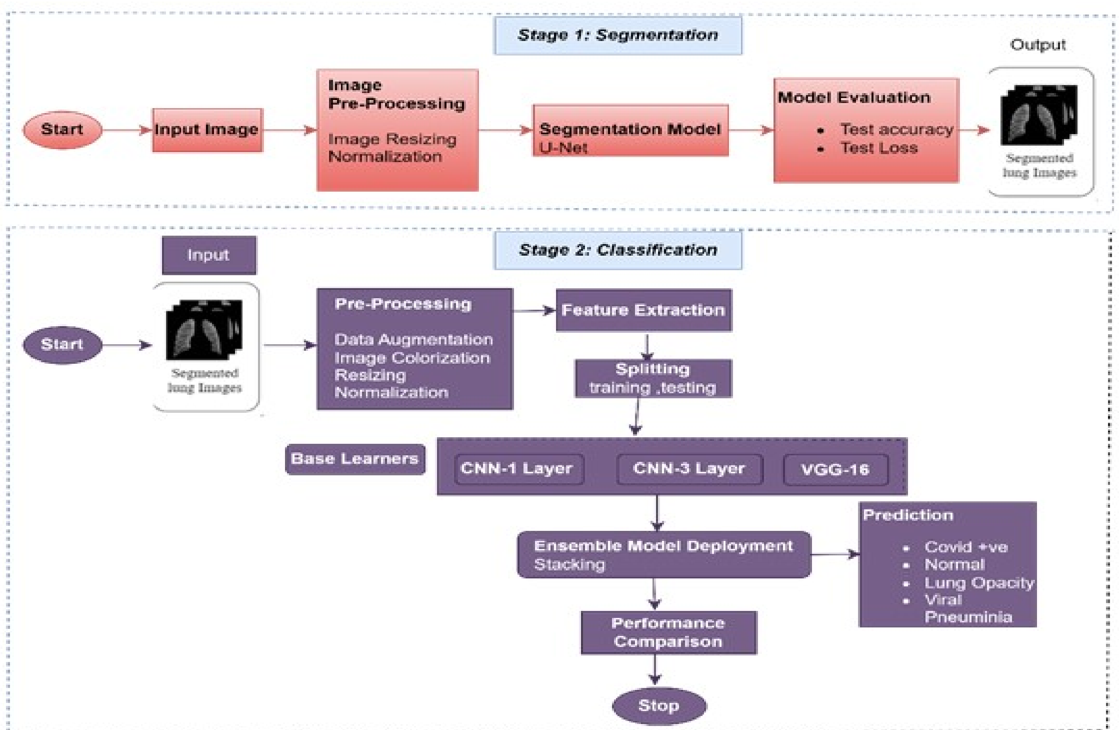


*Figure 8: Flowchart of the Ensemble learning framework.*

Figure 8. represents the flow process of implementation of a proposed framework with two phases: 1. Segmentation applied on the image set with U-Net model obtained segmented set of images; input to the 2nd phase. 2. Classification applied on CNN-1, CNN-3, VGG-16 along with some metrics to classify disease classes.

## 4. METHODOLOGY

a. CNN 1-Layer

The input tensor size is image height*width*channels, which is fed into this CNN.

Here, I set up the CNN to handle inputs of this size (256, 256, 3) from the earlier DIMENSIONS variable declaration.

- In the convolution operation, the first layer is a Conv2D layer, which creates a feature map by swiping a convolution filter over the input to extricate attributes from the input images.
- The max-pooling process's second layer is a MaxPooling2D layer that lowers the dimensionality of each feature, which contributes to a decrease in training time and parameter count.
- As the third layer, I include a Dropout layer, a potent regularization technique, to counteract overfitting.

*Table 2: CNN Layer 1 Architecture*

| **Input Layer** | **Activation Shape** | **#Parameter** |
|---|---|---|
| Conv2D | 256,256,32 | 856 |
| MaxPooling2D | 128,128,32 | 0 |
| Dropout | 128,128,32 | 0 |
| Flatten | (None, 556128) | 0 |
| Dense | 128 | 65,056,556 |
| Dense-1 | (None, 4) | 516 |
| Total parameters: 65,056,556 | | |
| Trainable parameters: 65,056,556 | | |
| Non-trainable parameters: 0 | | |

The dropout technique is employed to lessen overfitting. The learning phase involves random deactivation of neurons, which forces the model to learn multiple distinct representations of the same data. Twenty per cent of the neurons in this model will be randomly turned off by dropout. The final stage involves feeding the final output tensor into FC-fully connected layers, also referred to as dense layers. The current output of these densely connected classifiers is a 3D tensor, while the inputs are 1D vectors. I must first flatten the 3D outputs to 1D in order to create two dense layers on top of them. The last layer has a sigmoid activation and four outputs. The sigmoid activation allows me to compute the output based on the threshold.

Table 2 summarizes the used layers in CNN-1 Architecture, the shape of each output layer, and the parameters. Finally, it gives the overall parameters as well as the parameters that are trainable and non-trainable.

b. CNN 3-Layer

- The Batch Normalization layers scale and modify the activations to normalize the input layers. Batch normalization lessens the number of unit values related to hidden layer shift (covariance shift). Additionally, it enables a network's layers to learn slightly more separately from one another.
- An effective regularization method known as Dropout layers counteracts overfitting utilized. The dropout technique is employed to lessen overfitting. For instance, the first dropout layer randomly disables 25% of the outputs.
- This model consists of two Max-Pooling layers, six Batch Normalization levels, five Dropout layers, and four Conv2D layers.
- The last layer has a sigmoid activation and four outputs.

*Table 3: CNN Layer 3 Architecture*

| **Layer-type** | **Output Shape** | **Param #** |
|---|---|---|
| Conv2D | 256, 256, 32 | 996 |
| MaxPooling2D | 128, 128, 32 | 0 |
| Conv2D_1 | 128, 128, 64 | 18, 796 |
| MaxPooling2D_1 | 62, 62, 64 | 0 |
| Conv2D_2 | 64, 64, 128 | 63, 856 |
| MaxPooling2D_2 | 32, 32, 128 | 0 |
| Flatten | 114205 | 0 |
| Dense | 512 | 58,912,982 |
| Dropout | 512 | 0 |
| Dense_1 | 25 | 141,328 |
| Dropout_1 | 256 | 0 |
| Dense_2 | 4 | 256 |
| Total parameters: 58,912,982 | | |
| Trainable parameters: 58,912,982 | | |
| Non-trainable parameters: 0 | | |

Table 3 summarizes the used layers in CNN-3 Architecture, the shape of each output layer, and the parameters. Finally, it gives the overall parameters as well as the parameters that are trainable and non-trainable.

c. VGG-16

Let us credit VGG-16's magnificent capacity to recognize images, whose architecture was first developed. It is a deep convolutional neural model with 16 levels. In the present global circumstances, this imaging modality has been widely used for lung disease diagnosis, such as COVID-19.

Eight central convolutional, densely connected layers constituting VGG-16 are equally arranged sequentially. Tiny receptive fields (3x3") are apparatus that the network uses to identify detailed patterns in the input images by small and vast amounts of the data. The deep convolutional networks and multiple convolutional layers of the neural network help constructively capture the complex hierarchies [34]. Dense layers in the VGG-16 model at the end are essential for the operation, as they have more detailed elements and higher grouping and classification. In this regard, the layer chains contain the fully connected layers and soft activation layer to transform the features found in the convolutional layers into probability outputs. As a result, probabilities under possible classes are the output, which signifies the chances that the input image belongs to that class.

Considering its advanced architecture, VGG-16 has a reputation for capturing complex patterns and achieving the highest classification accuracy. VGG-16 can successfully recognize a range of lung affections, such as COVID-19, virus pneumonia, low lung density, etc., by virtue of its training on massive data of radiographs related to chest diseases.

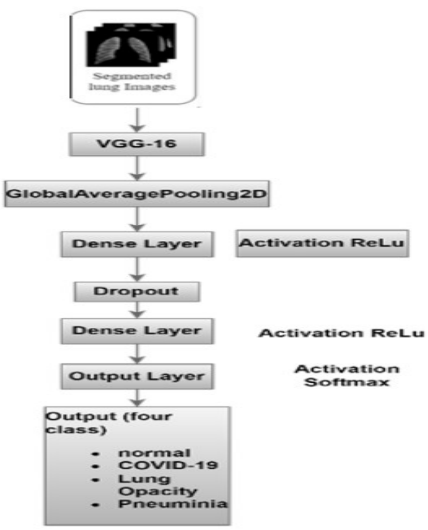


*Figure 9: VGG-16 Classification Model*

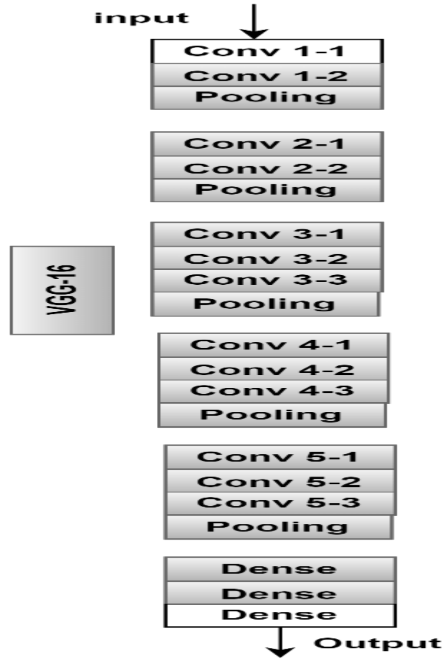


*Figure 10: VGG16 Architecture*

The above Figure 9 and 10 represent the VGG-16 Classification Model and Layer Architecture, which contains 16 layers, including 13 Conv layers and three fully connected l, which are dense layers.

**Hyper-Parameters**

a. Global Average Pooling2d

Image classification usually implements convolutional neural networks (CNN), as the Global average pooling (GAP) approach is used for the image classification function. It structures the abstract space of the input data into a smaller space, reducing overfitting. In this case, the path length will increase until it reaches the last average pooling layer of the network. Contrary to the general procedure of taking the mean of all the feature bits turned into one-dimensional vectors first, and then these vectors got mapped into the fully connected layers, GAP does not do this kind of transformation.

$$GAP(c) = \frac{1}{HxW} \sum_{i=1}^{H} \sum_{j=1}^{W} F(i, j, c) \quad \ldots (2)$$

b. Softmax Activation

The raw output of the neural network is transformed into a distribution format including the probability of several classes by one of the well-known activation functions, Softmax. The vector of real values is given to the mathematical function

Softmax as input; it scales the vector and forms a probability distribution with K probabilities according to the exponent of the original values.

Stated the inputting vector z = (z1,z2,...,zk), the softmax function computes the output vector σ(z) = (σ(z1),σ(z2),....,σ(zk)), where each element σ(zi) is calculated as:

$$\text{SoftMax}(Z_i) = \frac{e^{Z_i}}{\sum_{j=1}^{n} e^{Z_i}} \quad \dots (3)$$

c. Relu Activation

Almost everyone often uses one function called activation, the Rectified Linear Unit (ReLU), which is frequently employed, particularly in Conv Nets and DeepN Nets (DNNs). This nonlinearity will let the organization recognize reflexive patterns and links in the data more quickly. ReLU function multiplies input x and their element-wise maximum element by zero. Alternately, it keeps those positive feature values intact while mapping negative feature values to zero.

$$\text{ReLU}(x) = \max(0, x) \quad \dots (4)$$

d. Adam Optimizer

It is the best optimizer algorithm for learning rate, which is very popular in recent deep learning applications. Thus, it is a mix of RMSProp and AdaGrad, which are two perfect alternatives. The term "Adam" represents adaptive movie estimation. Adam keeps two moving averages set to zero vectors. However, they are also likely to be accompanied by (momentum) and (uncentered variance) undefined.

i. Locating the slope of the loss decision concerning the model parameters.
ii. Revision of Come-back time.

$$m_t = \beta_1 . m_{t-1} + (1 - \beta_1). g_t \quad \dots (5)$$

Where β1controls the exponential decay rate of the moving average of the gradient.

iii. Updating of the second moment estimate.

$$v_t = \beta_2 . v_{t-1} + (1 - \beta_2). g_t^2 \quad \dots (6)$$

Where β2 controls the exponential decay rate of the moving average of the squared gradient.

iv. Optimization of the estimates' bias

$$m_t^1 = \frac{m_t}{1-\beta_1^t} \quad \dots (7)$$

$$v_t^1 = \frac{v_t}{1-\beta_2^t} \quad \dots (8)$$

v. Modify the parameters where ε is practically around zero and η is referred to as the learning rate, a deficient number (say, 0.001).

The Adam optimizer, which is more or less the same as the SGD algorithm, assumes independent learning rates. Modifying each parameter independently will be the critical point to achieving better results and faster convergence compared to the other SGD algorithms. Through the facility to serve and recognition, it is often treated as a tool that accomplishes the purpose.

e. Loss Function

If the tasks need the multi-class classification, and the target labels are given as the integers that show the class by index, then a loss function of the sparse categorical cross entropy type is applied. Data and model gap: a sparse categorical cross entropy illustration, is depicted. Unlike the one-class versus all sample problem where sparse categorical cross-entropy outperforms, the multi-class case may demand other loss functions.

$$L(y, p) = -\frac{1}{n}\sum_{i=1}^{N}\sum_{j=1}^{C} y_{ij} \log(p_{ij}) \quad \dots (9)$$

**Segmentation**

Pre-processing

a. Image Resizing

The following resizes the images to the predefined size. This means that each picture will have the exact dimensions, i.e. width and height. "downscaling" the photographs to 256x256 means that all of them will have the fixed dimensions. This means that more outputs and information storage capabilities are needed to educate more giant neural nets and run the networks. The simplicity of the training and memory processing resource will ensure the competency of the achieved model. Therefore, it might be beneficial in terms of the model's efficiency.

b. Normalization

Normalization is the process of transforming an image that comprises pixel format conversion to a homogenous scale, in addition to handling situations that improve accuracy and computer performance. This produces an imitative, difficult training process in which only the strong factors decide the training procedure, whereas the rest of the input values have a reversed or opposite effect.

ISSN: 1992-8645 www.jatit.org E-ISSN: 1817-3195

c. UNet Model Development

It can perform chest disease segmentation in biomedical image analysis with an accuracy of 0.95. The convolutional part of the U-Net encodes the input image and extracts the contextual information. Layer 1 of the network is accountable for the downsized feature maps to catch the more abstract features, which is followed by the convolutional layers that consecutively apply filters to acquire feature maps. There is up-sampling with the U-Net decoder module and the skip link, which follows the up-sampling with the merge encoder feature maps and the up-sampled features.

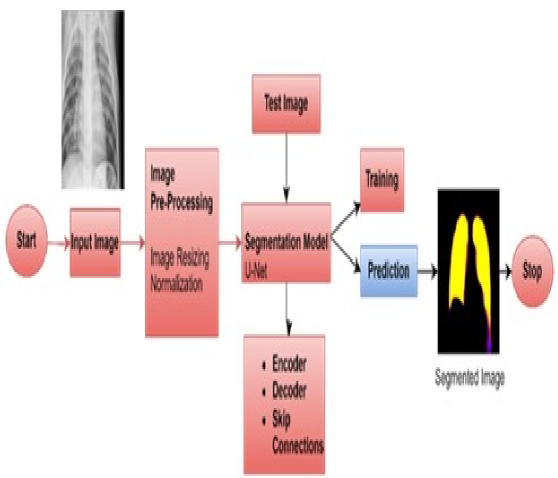


*Figure 11: Flow diagram of the segmentation*

Figure 11 utilizes the original data augmentation images and then applies pre-processing techniques, including resizing and normalization. It also applies the U-Net Segmentation model with Encoder, Decoder, and Skip Connections, generating a segmented set of images.

i. Encoder

In the "U-Net" architecture of image segmentation, the "encoder" is the part of the network that reads hierarchical features from the image. Through a spat of convolutional and pooling layers, the encoder keys both top-level semantic information and below-level details.

The encoder extracts feature at distinct degrees of abstraction and decimates the input image. That is, the process of segmenting data requires the network to correctly record and interpret both local details and global context. These circumstances allow it to occur.

ii. Decoder

The "decoder" of the U-Net architecture for image segmentation is the part that upsamples the encoder's feature maps, producing high-resolution segmentation masks. The decoder gradually refines the rough feature representations into detailed segmentation predictions, gradually restoring spatial information lost during the encoding process.

The number of up-sampling blocks defines the length of the decoder. The enhanced accuracy of segmentation with deeper decoders comes with the risk of overfitting, especially when the data used for training is less. The sampling process can be driven by the concatenation of encoder feature maps with the corresponding decoder level skip connections, and spatial information is made more detailed.

iii. Skip Connections

Connecting layers via skip connections in the decoding and encoding pathways directly affects the matching layers. This type of connection corrects information loss during the encoding route due to its low angular resolution. Skip connections provide a shortcut to a high-level path by giving access to high-reshaping feature maps from the preceding layers that may have otherwise been lost while down-sampling. Hence, this enables the network to regain lost spatial features.

d. Loss function

The Binary Cross-Entropy (BCE) loss function, which is also commonly known as Binary Logarithmic Loss or Sigmoid Cross-Entropy loss, is added in many binary levels categorizing tasks, for example, image segmentation, where the whole image is segmented into two kinds of pixel: foreground and background. BCE loss puts higher penalization when the estimated probability differs from the actual label. A deep cut will be the outcome if the actual label is 1, the predicted probability is close to 0, or the predicted label is 0, and the exact probability is close to 1. Suppose the predicted likelihoods of the events match with the proper labels. In that case, the loss is minimized, leading to more confident predictions of positive occurrences and less confident ones of negative ones.

Journal of Theoretical and Applied Information Technology
31st March 2025. Vol.103. No.6

ISSN: 1992-8645 www.jatit.org E-ISSN: 1817-3195

## 5. RESULT AND DISCUSSION

Evaluation metrics

a. Classification

We employ accuracy score, precision, recall and F1 score measures as performance metrics to evaluate the proposed classification model; we use

- TP (True Positives)- When a sample's actual label is positive, and the model predicts a positive outcome, this is known as a true positive (TP).
- TN (True Negatives)- count of accurately classified instances from the other classes.
- FP (False Positives)- count of inaccurately classified instances from the other classes.
- FN (False Negatives)- count of inaccurately classified instances of the targeted class.
- Accuracy can be determined by considering both positive and negative classes.

$$\text{Accuracy} = \frac{TP + TN}{TP + TN + FP + FN} \quad \cdots (10)$$

$$\text{Recall} = \frac{TP}{TP + FN} \quad \ldots (11)$$

$$\text{Precision} = \frac{TP}{TP + FP} \quad \ldots (12)$$

$$F1 - \text{Score} = \frac{2 * \text{Precision} * \text{Recall}}{\text{Precision} + \text{Recall}} \quad \ldots (13)$$

$$\text{Macro} - F1 = \text{average of F1 Scores} \quad \ldots (14)$$

$$\text{Weighted} - F1 = \text{Weighted} - \text{average of F1 Scores} \quad \ldots (15)$$

$$\text{Misclassification} = \frac{\text{incorrect predictions}}{\text{total predictions}} \quad \ldots (16)$$

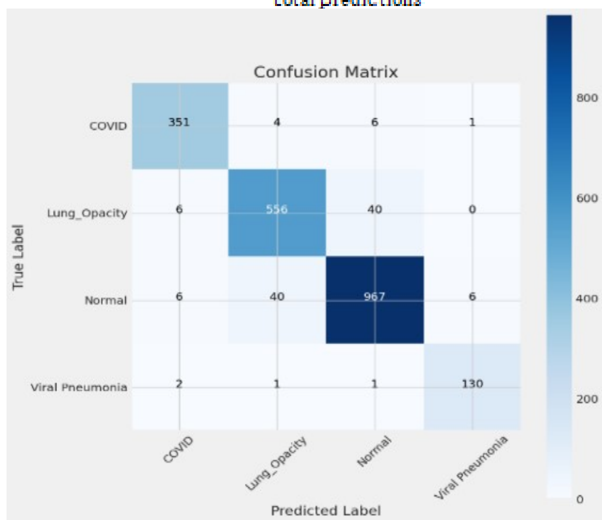


*Figure 12: Confusion matrix for the proposed Ensemble model*

*Table 4: Comparison of models with evaluation metrics*

| S. No | Model | NORMAL | | | COVID-19 | | | LUNG OPACITY | | | VIRAL PNEUMONIA | | |
|---|---|---|---|---|---|---|---|---|---|---|---|---|---|
| | | Precision | Recall | F1-score | Precision | Recall | F1-score | Precision | Recall | F1-score | Precision | Recall | F1-score |
| 1. | CNN-1 Layer | 90 | 95 | 93 | 94 | 94 | 94 | 92 | 83 | 87 | 95 | 95 | 95 |
| 2. | CNN-3 Layer | 93 | 94 | 93 | 91 | 94 | 92 | 90 | 87 | 89 | 94 | 94 | 94 |
| 3. | VGG-16 | 88 | 85 | 87 | 81 | 83 | 82 | 87 | 90 | 89 | 97 | 87 | 92 |
| 4. | ENSEMBLE | 95 | 95 | 95 | 96 | 97 | 97 | 93 | 92 | 92 | 95 | 97 | 96 |

*Table 5: Results of each model with accuracy score*

| S.No | Model | Accuracy |
|---|---|---|
| 1. | CNN-1 LAYER | 92 |
| 2. | CNN-3 LAYER | 93 |
| 3. | VGG-16 | 87 |
| 4. | ENSEMBLE | 96 |

Table 4 and 5 give a detailed analysis of four models: CNN-1 LAYER, CNN-3 LAYER, VGG-16, and ENSEMBLE, with four classes. Each class is compared with three metrics: precision, recall, and F1 score. The ensemble model performed exceptionally well, and the lung disease was predicted 96% accurately.

ISSN: **1992-8645** www.jatit.org E-ISSN: **1817-3195**

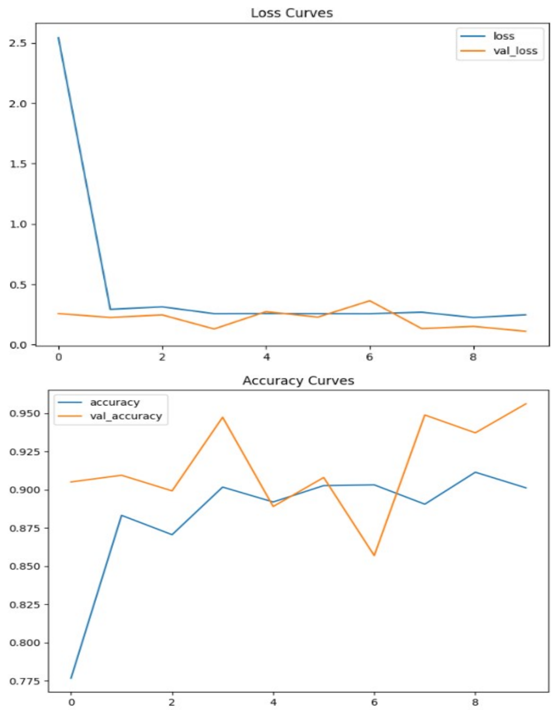


*Figure 13: CNN-1 Layer Accuracy and Loss*

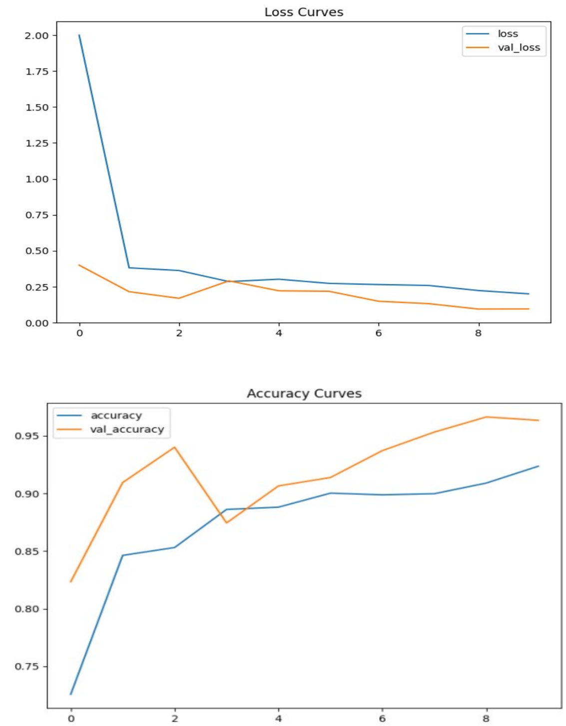


*Figure 15: Ensemble model Accuracy and Loss*

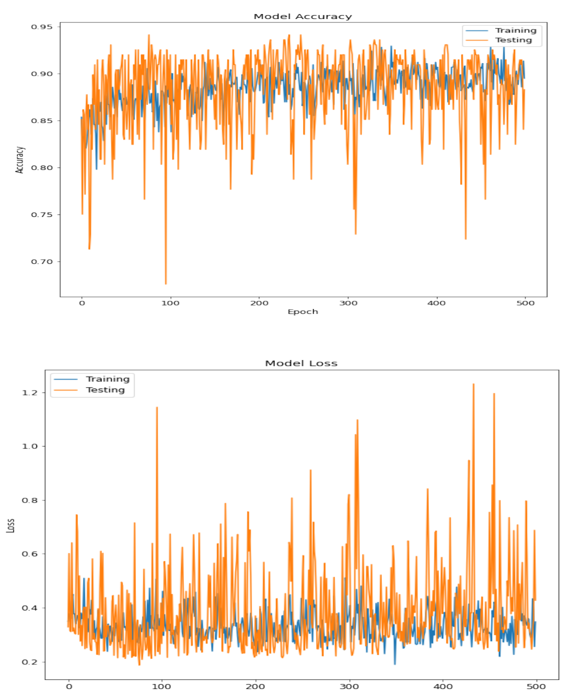


*Figure 14: CNN-3 Layer Accuracy and Loss*

Figures 13, 14, and 15 above show line graphs showing accuracy vs validation accuracy and loss vs validation loss for CNN-1, CNN-3, and Ensemble models, respectively.

b. Segmentation

Mean Intersection Over Union (Iou):

The overlap between each class's predicted segmentation mask and ground truth mask is measured using Mean IoU, which averages these IoU values across all classes. The intersection area (IoU) calculated a ratio of their union area with the base truth values and masks of the predicted part. Higher values indicate a more substantial overlap between the anticipated and ground truth masks. IoU values range from 0 to 1. Mean IoU offers a thorough assessment of segmentation accuracy for each class, accounting for the model's segmentation performance.

$$\text{Mean IOU} = \frac{1}{n}\sum_{i=1}^{n} \text{IOU}_i \quad \ldots \quad (17)$$

*Table 6: Metrics for U-Net model (segmentation)*

| Metrics | Training | Validation |
|---|---|---|
| Accuracy | 9.01% | 98.17% |
| Loss | 0.0234 | 0.0548 |
| Mean Iou | 0.6808 | 0.5704 |

c. Prediction

This research tested 21 thousand chest X-ray Radiograph images. It proposed an ensemble model with a combination of CNN-1, CNN-3 Layer, and VGG-16, which predicts the disease accurately in 96% of patients. The misclassification rate is very low, 0.04%.

*Table 7: Comparison of accuracies of existing Segmentation models and our model*

| Model | Accuracy | Total Images |
|---|---|---|
| Using Chest X-rays and Deep Learning for Segmentation and Visualization, TB Detection Is Reliable. TAWSIFUR RAHMAN | 98.20 | 8530 |
| COVID-19 Prediction Using Chest X-Ray Images and the COVIDGR Dataset and COVID-SDNet Methodology Tabik, S. | 74.60 | 9653 |
| COVID-19 Diagnosis Using Wavelets-Based Depthwise Convolution Network on Chest X-Ray Images Akansha Singh and Krishna Kant Singh | 96.53 | 12495 |
| Proposed Ensemble model | 98.17 | 21,165 |

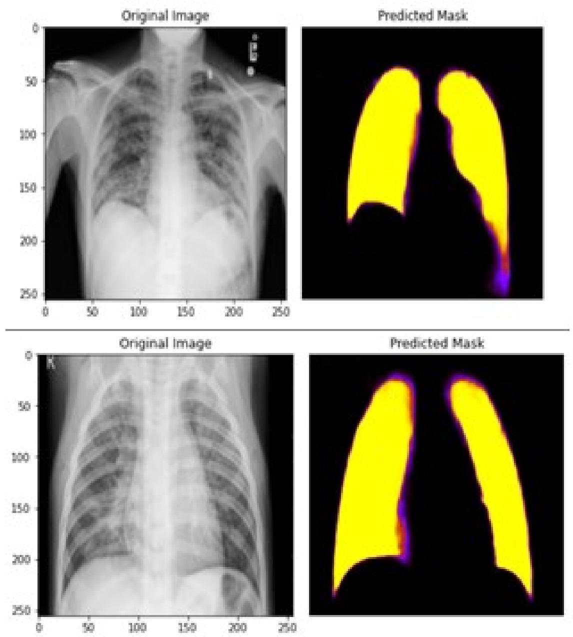


*Figure 16: Represents the original image and corresponding predicted segmentation mask*

## 6. CONCLUSION

Our investigation establishes a crucial advancement in diagnosing diabetic retinopathy by determining that a minimum image size of 28×28 pixels is necessary. This conclusion was reached after a comprehensive analysis of the magnitude spectrum, Nyquist frequency, and sinusoidal waveform properties. This advancement guarantees precise predictions even with lower-resolution images, thus enhancing the model's usability across diverse imaging techniques and resource-constrained environments. Moreover, employing improved ResNet and Dense Net algorithms on downscaled images yields favourable outcomes. By optimizing deep learning architectures for reduced image dimensions, we attain notable accuracy, sensitivity, and specificity in the classification of diabetic retinopathy while preserving computational efficiency. These data illustrate the successful attainment of our research objectives—creating an effective, scalable, and resource-efficient methodology for diabetic retinopathy screening. Furthermore, our methodology facilitates economical screening initiatives, especially in marginalized communities with restricted access to high-resolution imaging. Nonetheless, specific limits must be recognized. The research predominantly centres on a particular dataset, and discrepancies in actual clinical imaging may affect generalizability. Moreover, variances in image quality, noise interference, and discrepancies in camera settings may present hurdles to model performance. Subsequent research should investigate a broader range of datasets and sophisticated picture preparation methods to augment resilience and adaptability. Our methodology enhances diabetic retinopathy diagnosis and promotes the development of revolutionary image processing techniques and deep learning models specifically tailored for low-resolution data, thereby advancing medical image analysis.

## CONFLICTS OF INTEREST

The authors have no conflicts of interest to declare.

## REFERENCES

[1] Leander, M., Lampa, E., Rask-Andersen, A., Franklin, K., Gislason, T., Oudin, A., Svanes, C., Toren, K., & Janson, C, "Impact of anxiety and depression on respiratory symptoms". Respiratory Medicine, 108(11), 2014, 1594-1600. https://doi.org/10.1016/j.rmed.2014.09.007.

[2] Rogers, L. K., & Cismowski, M. J, "Oxidative stress in the lung – The essential paradox", Current Opinion in Toxicology, 7, 2018, 37-43. https://doi.org/10.1016/j.cotox.2017.09.001

[3] Solairaja, S., Mohideen, H., & Venkata Balasubramanian, S, "Computational Identification and Validation of Non-Synonymous SNPs in Progesterone Receptor Membrane Complex 1 Linked to Lung Cancer. Int. J. Exp. Res. Rev., 36, 2023,66-75. https://doi.org/10.52756/ijerr.2023.v36.006

[4] Issac, C., Sundaram, C., Narasimhan, M., & Rathinam, S, "Impact of Pulmonary Rehabilitation on Fatigue and Quality of Life in Patients of Interstitial Lung Disease", International Journal of Experimental Research and Review, 40(Spl Volume), 2024, 191-199. https://doi.org/10.52756/ijerr.2024.v40spl.016

[5] Roychoudhury, S., Das, A., Jha, N.K., Kesari, K.K., Roychoudhury, S., Jha, S.K., Kosgi, R., Choudhury, A.P., Lukac, N., Madhu, N.R., Kumar, D., & Slama, P, "Viral pathogenesis of SARS-CoV-2 infection and male reproductive health", Open Biology, 11, 2021, 200347.

[6] Deva, R., & Dagur, A, "A Novel Computer-Aided Approach for Predicting COVID-19 Severity Using Hyperparameters in ResNet50v2 from X-ray Images", International Journal of Experimental Research and Review, 42, 2024, 120-132. https://doi.org/10.52756/ijerr.2024.v42.011

[7] Sharma, K., Agarwal, S., & Singh, B, Queuing Theory-Based Model for Optimization of Covid-19 Vaccination and Booster Delivery. International Journal of Experimental Research and Review, 45(Spl Vol), 2024, 251–260. https://doi.org/10.52756/ijerr.2024.v45spl.020

[8] Paritala, A., Lakshmanan, M., Narasimhan, M., & Rathinam, S, "Evaluation of Pulmonary Status of Post-Tuberculosis Patients with Spirometry and Chest X-Ray", International Journal of Experimental Research and Review, 40(Spl Volume), 2024, 227–234.

[9] Singh, V. K., Abdel-Nasser, M., Pandey, N., & Puig, D, "LUNGINFSEG: Segmenting Based on a Receptive-Field-Aware Deep Learning framework, COVID-19 infected regions in lung CT images", Diagnostics, 11(2), 2021, 158. https://doi.org/10.3390/diagnostics11020158

[10] Liu, J., Dong, B., Wang, S., Cui, H., Fan, D., Ma, J., & Chen, G, "COVID-19 lung Infection segmentation with a novel two-stage cross-domain transfer learning framework", Medical Image Analysis, 74, 2021, 102205.

[11] Chauhan, S., Edla, D. R., Boddu, V., Rao, M. J., Cheruku, R., Nayak, S. R., Nigat, T. D, "Detection of COVID-19 using edge devices by a light-weight convolutional neural network from chest X-ray images". BMC Medical Imaging, 24(1), 2024. https://doi.org/10.1186/s12880-023-01155-7

[12] Asghar, M. Z., Albogamy, F. R., Al-Rakhami, M. S., Asghar, J., Rahmat, M. K., Alam, M. M., Nasir, H. M, "Facial mask detection using depth wise separable convolutional neural network model during the COVID-19 pandemic", Frontiers in PublicHealth,10,2022. https://doi.org/10.3389/fpubh.2022.855254

[13] Maheshwari, B. U., Sam, D., Mittal, N., Sharma, A., Kaur, S., Askar, S. S., & Abouhawwash, M, "Explainable deep-neural-network supported scheme for tuberculosis detection from chest radiographs", BMC Medical Imaging, 24(1), 2024. https://doi.org/10.1186/s12880-024-01202-x

[14] Saood, A., & Hatem, I, "COVID-19 lung CT image segmentation using deep learning methods: U-Net versus SegNet", BMC Medical Imaging, 21(1), 2021. https://doi.org/10.1186/s12880-020-00529-5

[15] Sun, W., Chen, J., Yan, L., Lin, J., Pang, Y., & Zhang, G, "COVID-19 CT image Segmentation method based on swing transformer", Frontiers in Physiology, 13, 2022.

[16] Al-Masni, M. A., & Kim, D, "CMM-Net: Contextual multi-scale multi-level network for efficient biomedical image segmentation", Scientific Reports,11(1),2021. https://doi.org/10.1038/s41598-021-89686-3

[17] Vasilev,Y., Vladzymyrskyy, A., Omelyanskaya, O., Blokhin, I., Kirpichev, Y., & Arzamasov, K, "AI-Based CXR First reading: Current limitations to ensure Practical value", Diagnostics, 13(8), 2023, 1430. https://doi.org/10.3390/diagnostics13081430

[18] Sahin, M. E., Ulutas, H., Yuce, E., & Erkoc, M. F, "Detection and classification of COVID-19 by using faster R-CNN and mask R-CNN on CT images", Neural Computing and Applications, 35(18), 2023, 13597–13611.

[19] Ippolito, D., Maino, C., Gandola, D., Franco, P. N., Miron, R., Barbu, V., Breaban, M. E, "Artificial intelligence applied to chest x-ray: a reliable tool to assess the differential diagnosis of lung pneumonia in the emergency department", Diseases, 11(4), 2023,171. https://doi.org/10.3390/diseases11040171

[20] Fung, D. L. X., Liu, Q., Zammit, J., Leung, C. K., & Hu, P, "Self-supervised deep Learning model for COVID-19 lung CT image segmentation highlighting putative causal relationship among age, underlying disease and COVID-19", Journal of Translational Medicine, 19(1), 2021. https://doi.org/10.1186/s12967-021-02992-2.

[21] Badrinarayanan, V., Kendall, A., & Cipolla, R, "SEGNet: a deep convolutional Encoder-Decoder architecture for image segmentation", IEEE Transactions on Pattern Analysis and Machine Intelligence, 39(12), 2017, 2481–2495. https://doi.org/10.1109/tpami.2016.2644615

[22] Alam, M., Wang, J., Guangpei, C., Yunrong, L., & Chen, Y, "Convolutional neural Network for the semantic segmentation of remote sensing images", Mobile Networks and Applications, 26(1), 2021, 200–215. https://doi.org/10.1007/s11036-020-01703-3

[23] Wu, M., Qian, Y., Liao, X., Wang, Q., & Heng, P, "Hepatic vessel segmentation-based on 3D swin-transformer with inductive biased multi-head self-attention", BMC Medical Imaging, 23(1), 2023. https://doi.org/10.1186/s12880-023-01045-y.

[24] Saha, A., & Yadav, R, "Study on segmentation and prediction of lung cancer based on machine learning approaches", Int. J. Exp. Res. Rev., 30, 2023,1-14.

[25] Gunraj, H., Wang, L., & Wong, A, "COVIDNet-CT: A tailored deep convolutional neural network design for detection of COVID-19 cases from chest CT images", Frontiers in Medicine, 7, 2020. https://doi.org/10.3389/fmed.2020.608525

[26] Kim, Y., Kim, K., Wu, D., Ren, H., Tak, W. Y., Park, S. Y., . . . Li, Q, "Deep Learning-Based Four-Region lung segmentation in chest radiography for COVID-19 diagnosis", Diagnostics, 12(1), 2022, 101. https://doi.org/10.3390/diagnostics12010101

[27] Afshar, P., Heidarian, S., Naderkhani, F., Oikonomou, A., Plataniotis, K. N., & Mohammadi, A, "COVID-CAPS: A capsule network-based framework for identification of COVID-19 cases from X-ray images", Pattern Recognition Letters, 138,2020,638–643. https://doi.org/10.1016/j.patrec.2020.09.010

[28] Khan, A. I., Shah, J. L., & Bhat, M. M, "CoroNet: A deep neural network for detection and diagnosis of COVID-19 from chest x-ray images", Computer Methods and Programs in Biomedicine, 196,2020,105581. https://doi.org/10.1016/j.cmpb.2020.105581

[29] Afshar, P., Mohammadi, A., & Plataniotis, K. N, "Brain Tumor Type Classification via Capsule Networks. 2018 25th IEEE International Conference on Image Processing (ICIP), 2018, pp. 3129–3133. https://doi.org/10.1109/icip.2018.8451379

[30] Bhalla, A. S., Jana, M., Naranje, P., & Manchanda, S, "Role of Chest Radiographs during COVID-19 Pandemic", Annals of the National Academy of Medical Sciences (India), 56(03), 2020, 138–144. https://doi.org/10.1055/s-0040-1714158 [31] Ye, Q., Xia, J., & Yang, G, "Explainable AI for COVID-19 CT Classifiers: An Initial Comparison Study", IEEE International Symposium on Computer-Based Medical Systems, 2021. https://doi.org/10.1109/cbms52027.2021.00103

[31] Ye, Q., Xia, J., & Yang, G, "Explainable AI for COVID-19 CT Classifiers: An Initial Comparison Study", *IEEE International Symposium on Computer-Based Medical Systems*, 2021. https://doi.org/10.1109/cbms52027.2021.00103

[32] Teixeira, L. O., Pereira, R. M., Bertolini, D., Oliveira, L. S., Nanni, L., Cavalcanti, G. D. C., & Costa, Y. M. G, "Impact of lung segmentation on the diagnosis and explanation of COVID-19 in chest x-ray images", Sensors, 21(21), 2021, 7116. https://doi.org/10.3390/s21217116

[33] Thimoteo, L. M., Vellasco, M. M., Amaral, J., Figueiredo, K., Yokoyama, C. L., & Marques, E, "Explainable artificial intelligence for COVID-19 diagnosis through blood test variables", Journal of Control Automation and Electrical Systems, 33(2), 2022, 625–644. https://doi.org/10.1007/s40313-021-00858-y

[34] Rao, Marada S.; Kumar, S.P.; Rao, Konda S, "A Methodology for Identification of Ayurvedic Plant Based on Machine Learning Algorithms", International Journal of Computing and Digital Systems, 14(1), 2023, 10233-10241. http://dx.doi.org/10.12785/ijcds/140196.